Cancer Research

H3K9 Histone Methyltransferase G9a Promotes Lung Cancer Invasion and Metastasis by Silencing the Cell Adhesion Molecule Ep-CAM

Min-Wei Chen[1], Kuo-Tai Hua[1], Hsin-Jung Kao[1], Chia-Chun Chi[1], Lin-Hung Wei[2], Gunnar Johansson[1], Shine-Gwo Shiah[6], Pai-Sheng Chen[1], Yung-Ming Jeng[3], Tsu-Yao Cheng[4], Tsung-Ching Lai[5], Jeng-Shou Chang[5], Yi-Hua Jan[5], Ming-Hsien Chien[8,9], Chih-Jen Yang[7], Ming-Shyan Huang[7], Michael Hsiao[5], and Min-Liang Kuo[1]

Abstract

G9a is a mammalian histone methyltransferase that contributes to the epigenetic silencing of tumor suppressor genes. Emerging evidence suggests that G9a is required to maintain the malignant phenotype, but the role of G9a function in mediating tumor metastasis has not been explored. Here, we show that G9a is expressed in aggressive lung cancer cells, and its elevated expression correlates with poor prognosis. RNAi-mediated knockdown of G9a in highly invasive lung cancer cells inhibited cell migration and invasion *in vitro* and metastasis *in vivo*. Conversely, ectopic G9a expression in weakly invasive lung cancer cells increased motility and metastasis. Mechanistic investigations suggested that repression of the cell adhesion molecule Ep-CAM mediated the effects of G9a. First, RNAi-mediated knockdown of Ep-CAM partially relieved metastasis suppression imposed by G9a suppression. Second, an inverse correlation between G9a and Ep-CAM expression existed in primary lung cancer. Third, Ep-CAM repression was associated with promoter methylation and an enrichment for dimethylated histone H3K9. G9a knockdown reduced the levels of H3K9 dimethylation and decreased the recruitment of the transcriptional cofactors HP1, DNMT1, and HDAC1 to the Ep-CAM promoter. Our findings establish a functional contribution of G9a overexpression with concomitant dysregulation of epigenetic pathways in lung cancer progression. *Cancer Res; 70(20); 7830–40. ©2010 AACR.*

Introduction

Aberrant DNA methylation is the primary epigenetic mechanism for regulating gene expression in human cancers (1, 2). Recent advances have shown that these DNA methylation changes are linked with the presence of an aberrant pattern of histone modification (3–7). This histone code (e.g., acetylation, methylation, phosphorylation, ubiquitinylation, and sumoylation), alone or together with DNA methylation, has a pivotal role in organizing nuclear architecture, which, in turn, is involved in regulating transcription. For example, DNA methylation is typically associated with heterochromatin and transcriptionally repressed euchromatic regions (8, 9). Current evidence suggests that H3K9 methylation and silencing of the $p16^{ink4a}$ tumor suppressor gene can occur before CpG methylation (10). Aberrant silencing of tumor suppressor genes *DSC3* and *MASPIN* in breast epithelial tumor cells has been previously linked to DNA methylation and H3K9 dimethylation of their promoters (11). It has been reported that changes in global levels of individual histone modifications are independently predictive of the clinical outcome of prostate cancer, gastric adenocarcinomas, as well as breast, ovarian, and pancreatic cancers (12–14). These results support the hypothesis that aberrant histone modification patterns are critically involved in the tumorigenic process.

G9a is a recently identified Su(*var*), Enhancer of *Zeste*, Trithorax (SET) domain–containing protein with histone lysine methyltransferase activity (15). G9a is a euchromatin-localized histone methyltransferase (HMT) and catalyzes the methylation of histone H3 at lysines 9 and 27 (H3K9 and K27; ref. 16). Targeted deletion of G9a in knockout mice revealed that G9a is predominantly responsible for

Authors' Affiliations: [1]Graduate Institute of Toxicology, National Taiwan University College of Medicine; Departments of [2]Oncology and [3]Pathology, National Taiwan University Hospital; [4]Department of Laboratory Medicine, National Taiwan University Hospital and National Taiwan University College of Medicine; [5]Genomics Research Center, Academia Sinica, Nankang, Taipei, Taiwan; [6]National Institute of Cancer Research, National Health Research Institutes, Miaoli, Taiwan; [7]Department of Internal Medicine, Kaohsiung Medical University Hospital, Kaohsiung Medical University, Kaohsiung, Taiwan; and [8]Taipei Medical University-Wang-Fang Hospital, and [9]Graduate Institute of Clinical Medicine, Taipei Medical University, Taipei, Taiwan

Note: Supplementary data for this article are available at Cancer Research Online (http://cancerres.aacrjournals.org/).

M-W. Chen and K-T. Hua contributed equally to this work.

Corresponding Authors: Min-Liang Kuo, Laboratory of Molecular and Cellular Toxicology, Institute of Toxicology, College of Medicine, National Taiwan University, No. 1, Section 1, Ren-ai Road, Taipei 100, Taiwan. Phone: 886-2-3970800 ext. 8607; Fax: 886-2-23410217; E-mail: kuominliang@ntu.edu.tw and Michael Hsiao, Genomics Research Center, Academia Sinica, Taipei 115, Taiwan. Phone: 886-2-27871243; Fax: 886-2-27899931; E-mail: mhsiao@gate.sinica.edu.tw.

doi: 10.1158/0008-5472.CAN-10-0833

dimethylation of H3K9 (H3K9me2; ref. 17). G9a plays an important role in the silencing and subsequent *de novo* DNA methylation of embryonic and germ-line genes during normal development (8) and is necessary for the maintenance of the DNA methylation profile of mammalian cells (9).

The role of HMTs in promoting tumorigenesis and the progression of human cancers has begun to emerge. Highly expressed EZH2 has been observed in metastatic prostate cancer, lymphomas, and aggressive breast cancer (18). SUZ12 is upregulated in some colon, breast, and liver cancers (19). G9a and EZH2 are also upregulated in hepatocellular carcinoma (20). The suppression of either G9a and SUV39H1 reduced cell proliferation and anchorage-independent colony growth while inducing apoptosis in immortalized normal human bronchial epithelial cells (21). Knockdown of G9a and SUV39H1 in PC3 prostate cancer cells inhibited cell growth and led to morphologically senescent cells with telomere abnormalities (22). These studies indicate that G9a seems to be required for the maintenance of the malignant phenotype.

Tissue invasion and metastasis are the major causes of cancer-related death (23). Some studies have found that HMTs specifically affect metastasis. EZH2 is linked to cell proliferation and invasion in prostate cancer and breast cancer (18, 24) and significantly associated with distant metastases in gastric cancer (25). A recent study further established a causal role for EZH2 in driving metastasis in prostate cancer (26). The functional roles of other members of the HMT family such as G9a in cancer remain obscure. Therefore, we investigated whether G9a might also function as a regulator of metastasis. In this report, we explore whether G9a represents a new metastasis promoter within the HMT family. We then define the mechanism by which G9a promotes metastatic lung cancer and show that epigenetic suppression of downstream Ep-CAM is an important mechanism by which G9a triggers metastasis. Furthermore, elevated levels of G9a correlate with poor prognosis and may act as an independent prognostic factor.

Materials and Methods

Specimens and immunohistochemistry

The tissues used were from the Cancer Tissue Core of the National Taiwan University Hospital. None of the patients had received preoperative neoadjuvant chemotherapy or radiation therapy. The surgical specimens had been fixed in formalin and embedded in paraffin before they were archived. We used the archived specimens for immunohistochemical staining. The histologic diagnosis of lung adenocarcinoma was made according to the recommendations of WHO. Tumor size, local invasion, lymph node metastasis, and final disease stage were determined as described previously (27). Follow-up of patients was carried out up to 200 months. Patients who died of postoperative complications within 30 days after surgery were excluded from the survival analysis.

A four-point staining intensity scoring system was devised for determining the relative expression of G9a in cancer specimens; the staining intensity score ranged from 0 (no expression) to 3 (maximal expression). The results were classified into two groups according to the intensity and extent of staining: in the low-expression group, either no staining was present (staining intensity score = 0) or positive staining was detected in less than 10% of the cells (staining intensity score = 1), and in the high-expression group, positive immunostaining was present in 10% to 30% (staining intensity score = 2) or more than 30% of the cells (staining intensity score = 3). All of the immunohistochemical staining results were reviewed and scored independently by two pathologists.

The antibodies included anti-human Ep-CAM (Cell Signaling Technology) and anti-G9a (R&D Systems, Perseus Proteomics). Immunodetection was performed with an EnVision dual link system-HRP detection kit (DAKO Corporation).

Cell culture

Lung cancer cell lines were grown in RPMI 1640 plus 10% fetal bovine serum (Invitrogen/Gibco) in a humidified atmosphere containing 5% CO_2 at 37°C. Lung adenocarcinoma cell lines (CL1-0 and CL1-5) were established in the National Health Research Institutes laboratory and displayed progressively increasing invasiveness (28). Other lung cancer cell lines (PC14, H441, and H1299) were obtained from the American Type Culture Collection.

Lentiviral infections

The lentiviral G9a shRNA constructs were purchased from the National RNAi Core Facility in Academic Sinica, Taipei, Taiwan. The Ep-CAM shRNA constructs were obtained from Open Biosystems. The target sequences of these shRNA are described in Supplementary Table S1. Lentiviruses were produced by cotransfecting shRNA-expressing vector and pMD2.G and psPAX2 constructs into 293T cells by using calcium phosphate. Viral supernatants were harvested, titered, and used to infect CL1-5 or H1299 cells with 8 μg/mL polybrene. Cells were selected using 2 μg/mL puromycin. Luciferase-expressing cells (CL1-0/Luc or CL1-5/Luc) were established by infecting with lentivirus-expressing pWPI-Luc-ires-GFP vector. CL1-0/HA-G9a cells were established by infecting with lentivirus-expressing pWPXL-HA-G9a vector.

Invasion and migration assays

Invasion and migration assays were performed as published (ref. 30; see Supplementary Data).

Western blot analysis

Western blot analysis was performed with the primary antibodies anti-G9a, anti-H3K9me2 (Upstate), anti–Ep-CAM (Cell Signaling Technology), and anti–α-tubulin (Sigma-Aldrich).

Animal studies

All animal works were done in accordance with a protocol approved by the National Taiwan University College of Medicine and National Taiwan University College of Public Health institutional animal care and use committees. Age-matched nonobese diabetic severe combined immunodeficient (SCID) female mice (6–8 weeks old) were used. For experimental metastasis assays, 1×10^6 cells were resuspended in 0.1 mL

of PBS and injected into the lateral tail vein. Lung metastatic progression was monitored and quantified using the noninvasive bioluminescence system (IVIS-Spectrum). For orthotopic metastasis assays, cells (1×10^6 CL1-0 cells, 5×10^5 CL1-5 cells) were resuspended in a 1:1 mixture of PBS and GFR-Matrigel (BD Labware). This mixture was then injected into the left lateral thorax of each mouse as previously described (29). Metastatic nodules in the right lung were quantified using a dissecting microscope at each end point.

Luciferase reporter assay

The *Ep-CAM* promoter (−250 to +90) was used as described (30). The Dual Luciferase Reporter assay system (Promega) was used with TK-Renilla luciferase plasmid as a transfection efficiency normalization control.

Chromatin immunoprecipitation assay

Chromatin immunoprecipitation (ChIP) assays were performed according to the manufacturer's protocol (Upstate). The chromatins were incubated with 4 μg of anti-K9 dimethylated histone H3, anti–acetylated histone H3, anti-G9a (Upstate), anti-DNMT1, anti-Sp1, anti-HDAC1, and anti-P300 antibody (Santa Cruz Biotechnology) at 4°C overnight. Immunoprecipitated DNA was analyzed by quantitative PCR by using specific primers as described in Supplementary Table S2.

Methylation-specific PCR and bisulfite sequencing

DNA was treated with bisulfite and purified for PCR as described previously (31). Primer sequences were as described in Supplementary Table S2. The sequences of the Ep-CAM promoter primers were 5-AAGGAAGTTTTAGTATAGAATTTTTAAATT-3 (F) and 5-AAAAAAATAAATAAACTCCCCTCC-3 (R). The PCR products were ligated into pGEM-T vector (Promega) and transformed into DH5α. Plasmid DNA was isolated and then subjected to sequence analysis.

Histopathologic analysis

Tissues were processed by fixing in 4% buffered formalin and then embedding in paraffin wax. Sections (3 μm) were stained with H&E for histopathologic analysis.

Statistical analysis

All observations were confirmed by at least three independent experiments. The data were presented as mean ± SD. ANOVA was used to evaluate the statistical significance of the mean values. Cox proportional hazards regression was used to test the prognostic significance of factors in univariate and multivariate models. Spearman's rank correlations were determined for comparison of G9a and Ep-CAM immunostaining. All statistical tests were two-sided, and $P < 0.05$ was considered significant.

Results

G9a expression in lung cancer is associated with poor prognosis

Comparisons of the expression levels of G9a in tumor tissues and control normal tissues were made. Immunohistochemical examination of 32 paired lung adenocarcinoma specimens revealed a significantly higher expression of G9a in tumor tissues ($P < 0.0001$; Supplementary Fig. S1). Similar results were also observed from the analysis of 22 paired lung squamous cell carcinoma specimens ($P < 0.0001$; Supplementary Fig. S1). Collectively, G9a was expressed at a lower level in normal lung tissues and preferentially expressed in lung tumor tissues.

The prognostic significance of G9a expression was determined by assessing its nuclear staining using 160 human lung cancer specimens with known clinical follow-up records. Figure 1A shows representative examples with different G9a scores. The relationships between the levels of G9a expression and the clinicopathologic characteristics of lung cancer are summarized in Supplementary Table S3. Among these specimens, we found that high G9a expression level (scores of 2 and 3) correlated strongly with reduced overall survival relative to tumors with low G9a expression level (scores of 0 and 1) as shown in Fig. 1B. Similar results were obtained for disease-free interval (Fig. 1C). The prognostic significance of G9a was also performed by using tissue microarray (TMA) containing 119 cases from an independent lung cancer patient cohort. Similar results were observed (Supplementary Fig. S2A; Supplementary Table S4). In a multivariate Cox model including G9a score, histology type, tumor stage, tumor status, lymph node involvement, and metastasis, G9a levels and metastasis were found to be significant predictors of outcome (Table 1; Supplementary Fig. S2B). Taken together, our data indicate that higher levels of G9a predict poor prognosis in lung cancer.

G9a expression enhances the invasive ability of lung cancer cells

To elucidate a link between G9a expression and tumor cell invasiveness, we used a set of lung adenocarcinoma cell lines (CL1-0 and CL1-5) that were designed to exhibit progressive invasiveness abilities as previously described (28). Western blot analysis showed that G9a protein levels were significantly elevated in the highly invasive CL1-5 lung cancer cells as compared with the poorly invasive parental CL1-0 cells (Fig. 2A, left). Next, we asked whether a correlation between G9a expression and tumor cell invasiveness occurred in other cell lines. We observed abundant G9a expression in the highly invasive H1299 lung cancer cell line, but low G9a expression in poorly invasive lung cancer cell lines (PC14 and H441; Fig. 2A, right). G9a and GLP have been described to form a homomeric or heteromeric complex through their SET domain interaction, both of which are crucial for H3K9 methylation of euchromatin (32). We also examined GLP expression and global H3K9me2 in these lung cancer cell lines. Our results showed similar levels of GLP expression in all cell lines tested but different levels of G9a expression (Fig. 2A). Global H3K9me2 status was not completely correlated with G9a expression in lung cancer cell lines (Fig. 2A).

To determine whether G9a modulates tumor cell migration and invasion, we knocked down G9a in CL1-5 and H1299 cells

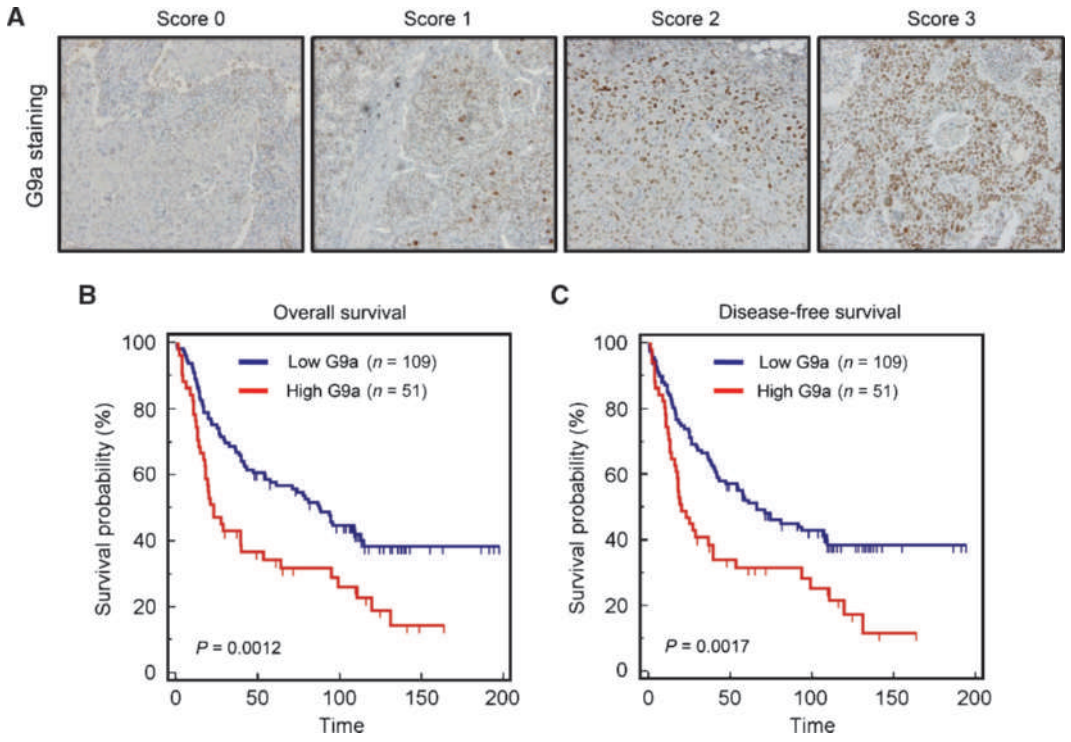

Figure 1. G9a is expressed in tumors and is correlated with poor prognosis. A, G9a levels in representative lung tumor tissues. B, Kaplan-Meier plot of overall survival of 160 patients with lung cancer, stratified by G9a level. C, Kaplan-Meier plot of disease-free survival of 160 patients with lung cancer, stratified by G9a level.

using G9a-specific shRNAs. We initially determined the influence of G9a knockdown on cell proliferation, apoptosis, and senescence as previously described (21, 22). Our results showed that G9a-knockdown cells exhibited no significant differences in proliferation, cell cycle, and senescence profiles as compared with controls (Supplementary Fig. S3A–D).

Interestingly, expression of two G9a-specific shRNAs significantly reduced the mRNA and protein levels of G9a with concomitant inhibition of the migration and invasion potentials of CL1-5 and H1299 cells (Fig. 2B; Supplementary Fig. S4). Overexpression of G9a in poorly invasive CL1-0 cells was also found to enhance the migratory and invasive

Table 1. Relative multivariate analysis of potential prognostic variables

		Multivariate analysis	
Parameters	**Comparison**	**HR (95% CI)**	***P***
G9a score	Low (score 0, 1); high (score 2, 3)	2.20 (1.44–3.38)	0.0003*
Histology type	Adenocarcinoma; nonadenocarcinoma	0.75 (0.48–1.16)	0.199
Pathologic stage	pT1–pT2; pT3–pT4	1.45 (0.80–2.63)	0.218
Tumor status	T1–T2; T3–T4	0.60 (0.30–1.20)	0.152
Lymph node status	NO; N1–N3	2.49 (1.52–4.06)	0.0003
Metastasis	MO; M1	2.37 (1.14–4.92)	0.022

NOTE: Cox proportional hazards regression was used to test the independent prognostic contribution of G9a after accounting for other potentially important covariates.
Abbreviations: HR, hazard ratio; CI, confidence interval.
*Two-sided Cox proportional hazards regression using normal approximation.

abilities of CL1-0 cells (Fig. 2B, right). G9a knockdown in A549 cells with lower endogenous G9a expression was also found to significantly inhibit their migration abilities (Supplementary Fig. S5). Taken together, these results indicate that G9a regulates the migration and invasion of lung cancer cells.

To determine whether the enzymatic activity of G9a was required for its effect in promoting cancer cell motility and invasion, CL1-5 and H1299 cells were transfected with a dominant-negative mutant of G9a (DN-G9a) containing two amino acid substitutions within the catalytic domain (N903H and L904E), which abolishes methyltransferase activity (33, 34). Figure 2C shows that DN-G9a transfection significantly reduced H3K9me2 level in CL1-5 and H1299 cells and inhibited their migratory and invasive abilities. On the basis of these results, we suggest that the HMT activity of G9a is required for the migratory and invasive phenotype of lung cancer cells.

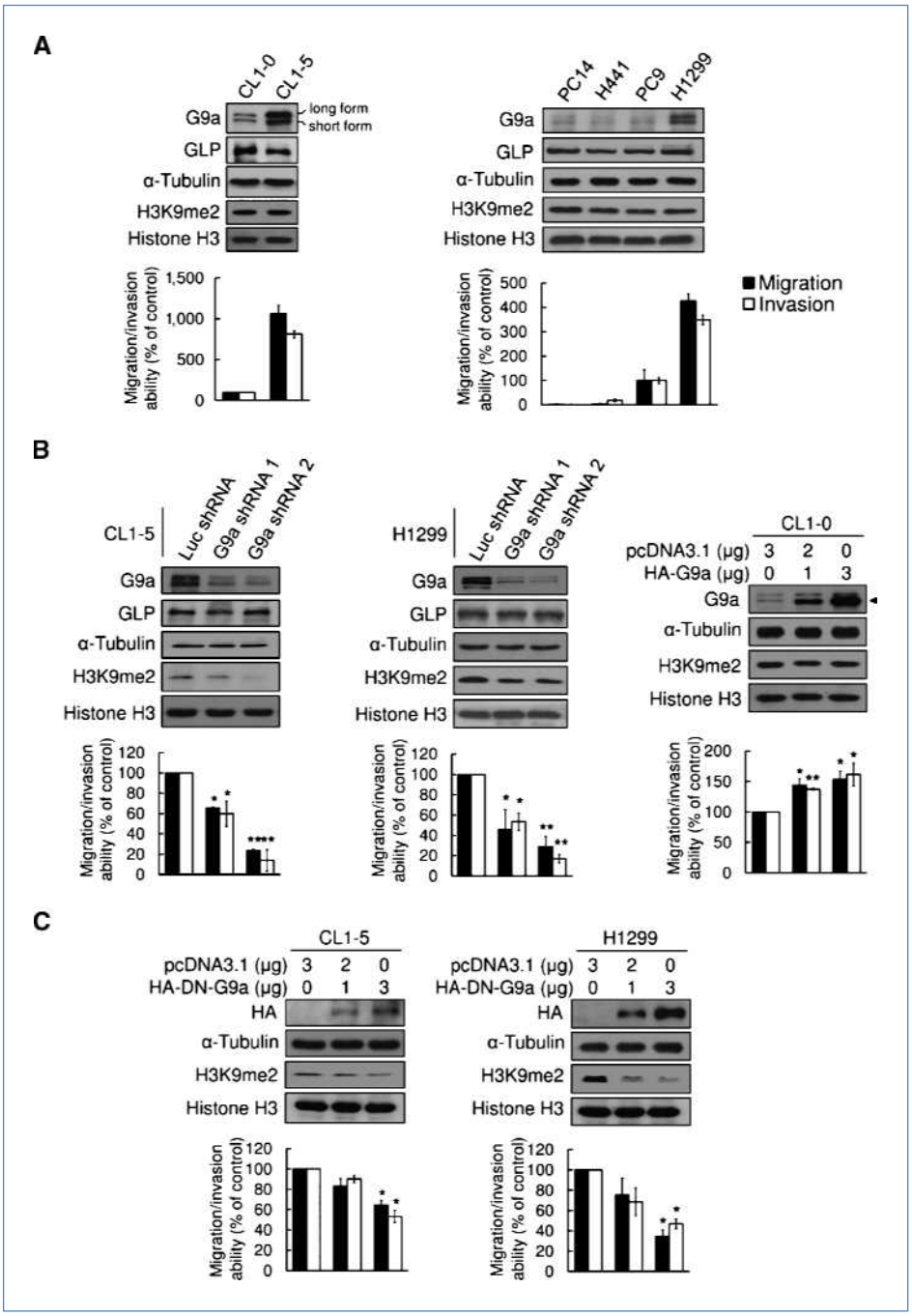

Figure 2. G9a expression enhances the invasive ability of lung cancer cells. A, endogenous G9a protein expression and *in vitro* migratory/invasive abilities of human lung adenocarcinoma cell lines. Top, Western blot analysis of G9a and its associated proteins, GLP and H3K9me2, in CL1-0 and CL1-5 cells (left) or PC14, H441, PC9, and H1299 cells (right). Bottom, migratory/invasive abilities of CL1-0 and CL1-5 cells (left) or PC14, H441, PC9 and H1299 cells (right). B, G9a knockdown and migratory/invasive abilities of lung cancer cells. Top, Western blot analysis of G9a expression in CL1-5 (left) and H1299 (middle) cells expressing G9a shRNA or in CL1-0 cells expressing HA-G9a (right). Bottom, migratory/invasive abilities of CL1-5 (left) and H1299 (middle) cells expressing G9a shRNA or of CL1-0 cells expressing HA-G9a (right). C, effect of G9a enzyme activity on the migratory/invasive abilities of CL1-5 and H1299 cells. Top, Western blot analysis of G9a expression in DN-G9a–transfected CL1-5 (left) or H1299 cells (right). Bottom, migratory/invasive abilities of DN-G9a–transfected CL1-5 (left) or H1299 cells (right).

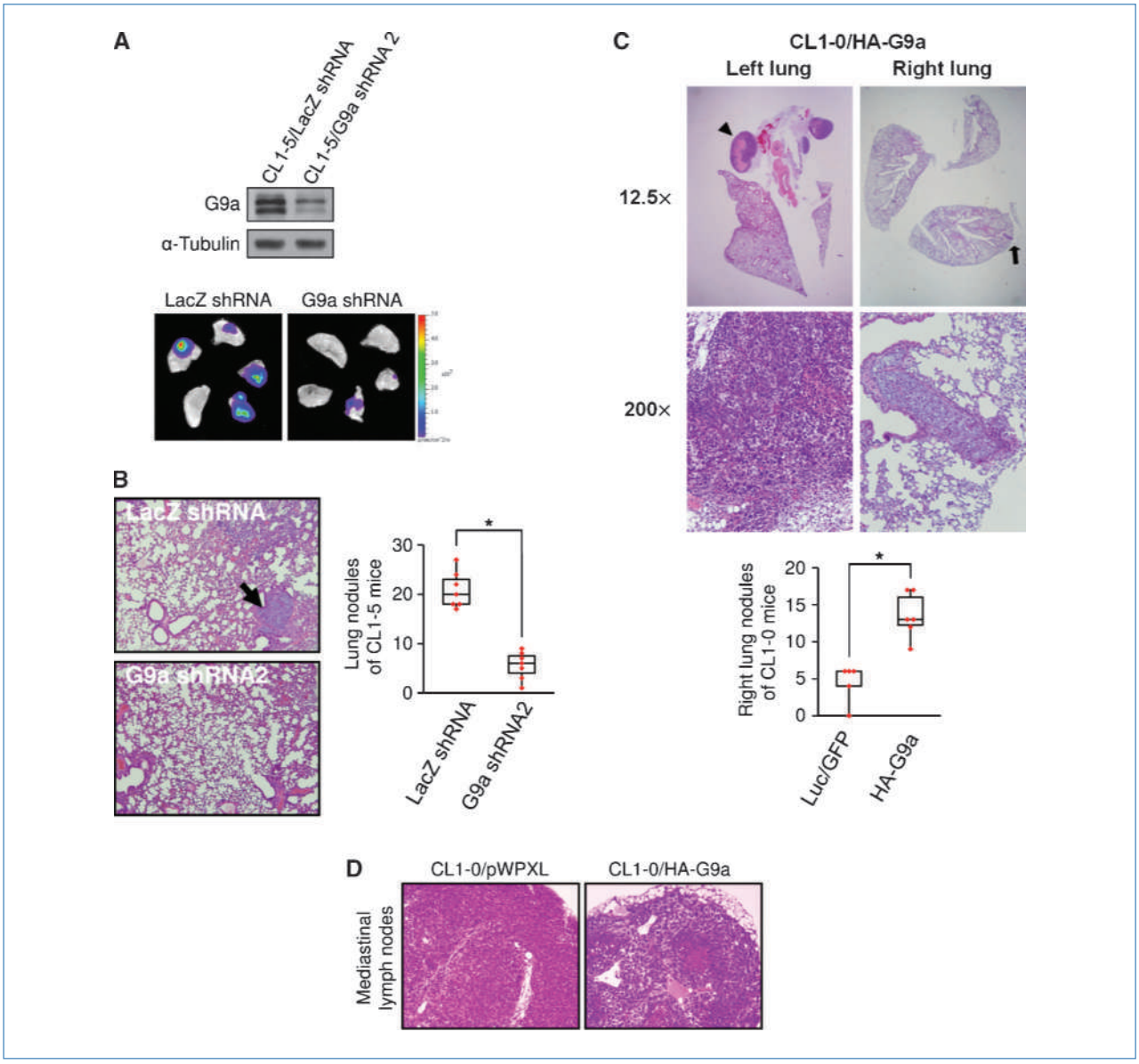

Figure 3. G9a expression promotes metastasis *in vivo*. A, top, expression of G9a protein was examined by immunoblotting in CL1-5 cells stably expressing control shRNA or G9a shRNA2. Bottom, representative lung images of mice injected with control and G9a shRNA2–expressing cells. The color bar represents luciferase intensity. B, left, representative H&E staining of lung sections. Black arrow, a metastatic nodule. Right, total numbers of lung metastatic nodules in individual mice 4 wk after tail vein injection of CL1-5 cells transfected with control shRNA or G9a shRNA2. C, top, representative H&E staining of left and right lung sections. Black arrowhead, the original CL1-0/HA-G9a tumor established in the left lung. Black arrow on the right lung shows an intrapulmonary metastatic tumor nodule. Bottom, total numbers of lung metastatic nodules in individual mice 4 wk after left lung orthotopic injection of CL1-0 cells transfected with control vector or HA-G9a vector. D, H&E microscopic photographs of the mediastinal lymph node. CL1-0/HA-G9a cancer cells invade into the center of the lymph node (right; 200×) as compared with the normal lymph node (left; 200×).

G9a expression promotes metastasis *in vivo*

To evaluate the role of G9a during metastasis, we used an experimental metastasis model in which cancer cells were i.v. injected into the lateral tail veins of mice. As shown in Fig. 3A, we stably knocked down G9a in CL1-5/Luc cells, which stably expressed luciferase, and implanted these cells i.v. into SCID mice (Fig. 3A). Four weeks after injection, the lung was removed and metastasis was monitored by bioluminescence imaging. G9a knockdown resulted in less detectable lung metastases compared with controls (Fig. 3A, right). Quantification of the metastatic nodules present using dissecting microscopy and histologic analyses of the lung dissected from each mouse confirmed that the number of lung metastases was drastically reduced in mice carrying G9a-knockdown tumors (Fig. 3B).

We next investigated whether ectopic expression of G9a is sufficient to induce invasive activity in low-metastatic cancer cells using an orthotopic lung cancer model as described (29). Low-metastatic CL1-0 cells stably expressing G9a were orthotopically injected into the upper lobe of left lung; tumor growth and metastasis were monitored and quantified by bioluminescence imaging. Tumor metastasis into the right lung was increased in the G9a-overexpressing group (Supplementary Fig. S6A). Quantification of metastatic nodules confirmed that right lung metastasis was significantly increased in mice carrying CL1-0/HA-G9a tumors (Fig. 3C). Overexpression of G9a did not alter *in vivo* tumor growth rate (Supplementary Fig. S6B). Furthermore, G9a-overexpressing CL1-0 cells were found to invade into mediastinal lymph nodes (Fig. 3D). Hence, G9a function is essential and sufficient to promote lung cancer metastasis.

Ep-CAM is a direct and functional target in G9a-induced migration and invasion

Microarray RNA expression profiles were compared between CL1-5 cells with control shRNA and G9a shRNA2 to identify invasion/migration-related genes directly regulated by G9a. Reverse transcription-PCR analysis was used to further validate the expression levels of these genes (Supplementary Fig. S7A). Our results showed that the mRNA levels of E-cadherin and Ep-CAM were significantly upregulated in G9a-knockdown cells compared with control (Supplementary Fig. S7A). E-cadherin and Ep-CAM protein levels were then determined in G9a-knockdown CL1-5 and H1299 cells. G9a knockdown significantly increased Ep-CAM protein levels in CL1-5 (7.5- and 16-fold) and H1299 cells (2.4- and 3.6-fold; Fig. 4A), whereas endogenous E-cadherin protein levels were extremely low in both cell lines. G9a knockdown induced low level of E-cadherin expression in CL1-5 but not

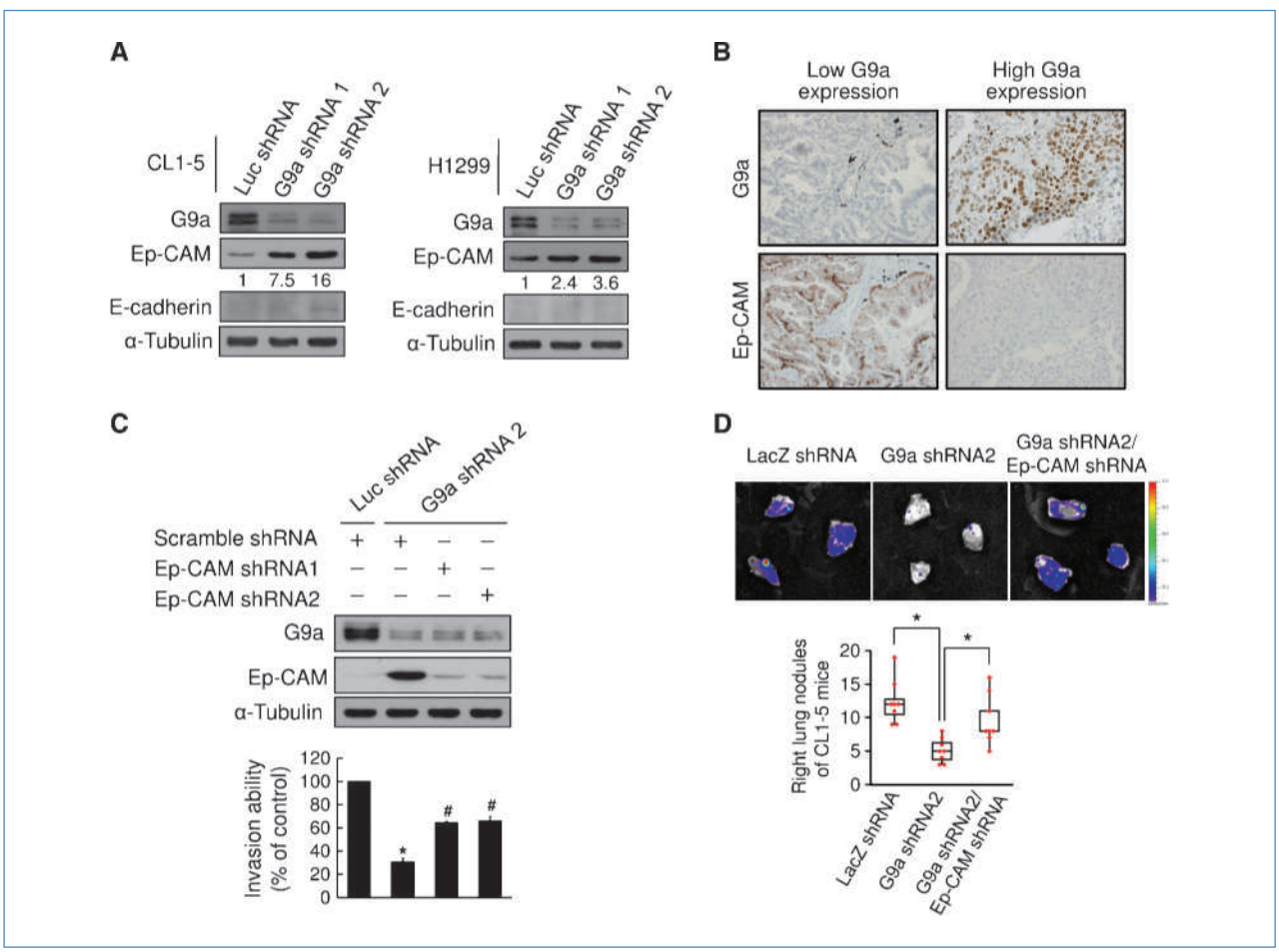

Figure 4. Ep-CAM is a direct and functional target in G9a-induced migration and invasion. A, Western blot analysis of Ep-CAM, E-cadherin, and G9a protein expression in G9a-knockdown CL1-5 (left) and H1299 (right) cells. B, immunohistochemical staining analysis of G9a and Ep-CAM proteins in serial sections. Note inverse correlation of G9a and Ep-CAM protein expression in tumor cells. C, top, Western blot analysis of G9a and Ep-CAM expression levels. Bottom, invasive ability of each cell line after G9a and/or Ep-CAM knockdown. D, top, representative luciferase images of mouse lung injected with G9a- and/or Ep-CAM–knockdown CL1-5 cells. Bottom, total numbers of right lung metastatic nodules in individual mice 4 wk after orthotopic injection of G9a- and/or Ep-CAM–knockdown CL1-5 cells.

in H1299 cells (Fig. 4A). Microarray RNA expression profiles were also determined in G9a-overexpressing CL1-0 cells and vector control. The results showed inverse correlation of RNA expression with G9a knockdown (Supplementary Fig. S7A). Western blot analysis further confirmed that ectopic overexpression of G9a induced a more than 2-fold reduction of 3Ep-CAM protein level in CL1-0 cells (Supplementary Fig. S7B).

We next investigated whether G9a expression inversely correlated with Ep-CAM levels in human lung cancer patients. Immunohistochemistry analysis of lung cancer specimens revealed an inverse correlation between G9a and Ep-CAM expression (tested by Spearman's nonparametric correlation test, correlation coefficient = –0.4, $P < 0.05$; Supplementary Table S5). The representative immunohistochemical staining for Ep-CAM and G9a on serial sections revealed inverse staining patterns in lung adenocarcinoma tissues (Fig. 4B). To extend the inverse correlation between G9a and Ep-CAM in human lung cancer, we further determined Ep-CAM levels in serial lung cancer TMA set in which G9a was examined. The results also revealed an inverse correlation between G9a and Ep-CAM expression (tested by Spearman's nonparametric correlation test, correlation coefficient = –0.189, $P < 0.05$; Supplementary Fig. S8A). The correlation of high G9a expression with low Ep-CAM expression in human lung cancer patients is consistent with our finding that knockdown of G9a can upregulate Ep-CAM in lung cancer cells.

These observations led us to examine whether Ep-CAM could reverse G9a-mediated phenotypes. As shown in Fig. 4C and Supplementary Fig. S9, infection and expression of two shRNAs significantly reduced the levels of Ep-CAM mRNA and protein with concomitant increase in the invasive ability *in vitro* of CL1-5 cells that were prior infected with G9a shRNA compared with control (Fig. 4C). To investigate whether Ep-CAM knockdown could reverse the *in vivo* metastatic phenotypes attributed to G9a functions, we orthotopically injected mice with CL1-5 cells expressing combinations of G9a shRNA, Ep-CAM shRNA, and control vector. G9a knockdown showed more than 70% reductions in total luciferase counts ($P < 0.05$) in orthotopic tumors (Supplementary Fig. S10). Ep-CAM shRNA, however, could abate primary tumor growth reduction in the presence of G9a shRNA (Supplementary Fig. S10). Ep-CAM knockdown was found to restore lung metastasis in G9a shRNA2–expressing CL1-5 cells to 77% of control levels in orthotopic left to right lung metastasis assay (Figs. 3C and 4D). Taken together, these data indicate that the ability of G9a shRNA to inhibit metastasis is attributable, in significant part, to its capacity to upregulate Ep-CAM.

G9a induces the assembly of a repressor complex at the *Ep-CAM* promoter

To further characterize the mechanism of G9a-mediated downregulation of Ep-CAM expression, we next examined G9a binding and H3K9 dimethylation at different regions of the human *Ep-CAM* gene by using ChIP analysis with antibodies against G9a and dimethyl-H3K9 (H3K9me2). Four representative regions spanning ~2.5 kb upstream of the transcription initiation site of the *Ep-CAM* gene were investigated (Fig. 5A, top). The results showed that G9a and H3K9me2 were found in region P3 only in CL1-5 cells (Fig. 5A). This region also contains a consensus binding site for Sp1, a transcription factor that has been reported to regulate *Ep-CAM* transcription activity (35). To delineate the role of Sp1 in G9a knockdown–mediated *Ep-CAM* transactivation, we transfected CL1-5 cells with shRNAs against Sp1 that have been previously infected with either Luc or G9a shRNA. Figure 5B shows that G9a knockdown resulted in a significant induction of the *Ep-CAM* promoter (–250/+90) luciferase activity (lane 2 versus lane 4), which was diminished in the presence of mithramycin A (a steric inhibitor that prevents Sp1 binding to DNA) or Sp1 shRNA, but not in the presence of P50 shRNA (lanes 4–9; Fig. 5B). These results suggest that G9a-regulated *Ep-CAM* gene transactivation is dependent on an endogenous Sp1 transcription factor.

To elucidate the assembly of the repressor protein complex that binds to the *Ep-CAM* promoter, we performed ChIP assay of the *Ep-CAM* promoter in G9a-knockdown CL1-5 cells and control. As expected, loss of G9a resulted in loss of H3K9me2, HP1, DNMT1, and HDAC1 binding at region P3 compared with SP1 (Fig. 5C). Methylation-specific PCR (MS-PCR) and bisulfite sequencing were further performed to evaluate whether G9a-knockdown is responsible for CpG demethylation of the *Ep-CAM* promoter. As shown in Fig. 5D, a clear unmethylated band of the *Ep-CAM* promoter was observed in G9a shRNA2–expressing CL1-5 cells by MS-PCR analysis (Fig. 5D, top). Bisulfite sequencing results confirmed that G9a knockdown significantly reduced *Ep-CAM* promoter methylation (Fig. 5D, bottom row). These results indicate that both DNA and histone methylation, along with repressive complexes, mediate *Ep-CAM* gene repression.

Discussion

HMT can act as a driver of metastasis (26). Here, we propose for the first time that G9a acts as a promoter of metastasis in the context of lung cancer. G9a is a major HMT that maintains global H3K9me2. Several studies have shown that lower global levels of H3K9me2 predict poor prognosis in prostate and kidney cancers (36, 37). Therefore, we analyzed the correlation between G9a and H3K9me2 level in human lung cancer TMA. We did not observe any significant correlation of G9a expression and global H3K9me2 level (Supplementary Fig. S12A). Global levels of H3K9me2 also did not predict prognosis in lung cancer (Supplementary Fig. S12B). We also found that global H3K9me2 level was not correlated with G9a expression in lung cancer cell lines (Fig. 2A). Global H3K9me2 is dynamic, and it changes as a result of the effects G9a, GLP, and H3K9 demethylases, such as JMJD2A (38), JMJD2C (39), and LSD1 (40), but the complex interplay of these enzymes is poorly understood. Based on our studies, G9a level is a more rigorous marker for cell invasion and prognosis factor in lung cancer. This may be due to the G9a suppression of transcription by independently inducing both H3K9 and DNA methylation (41).

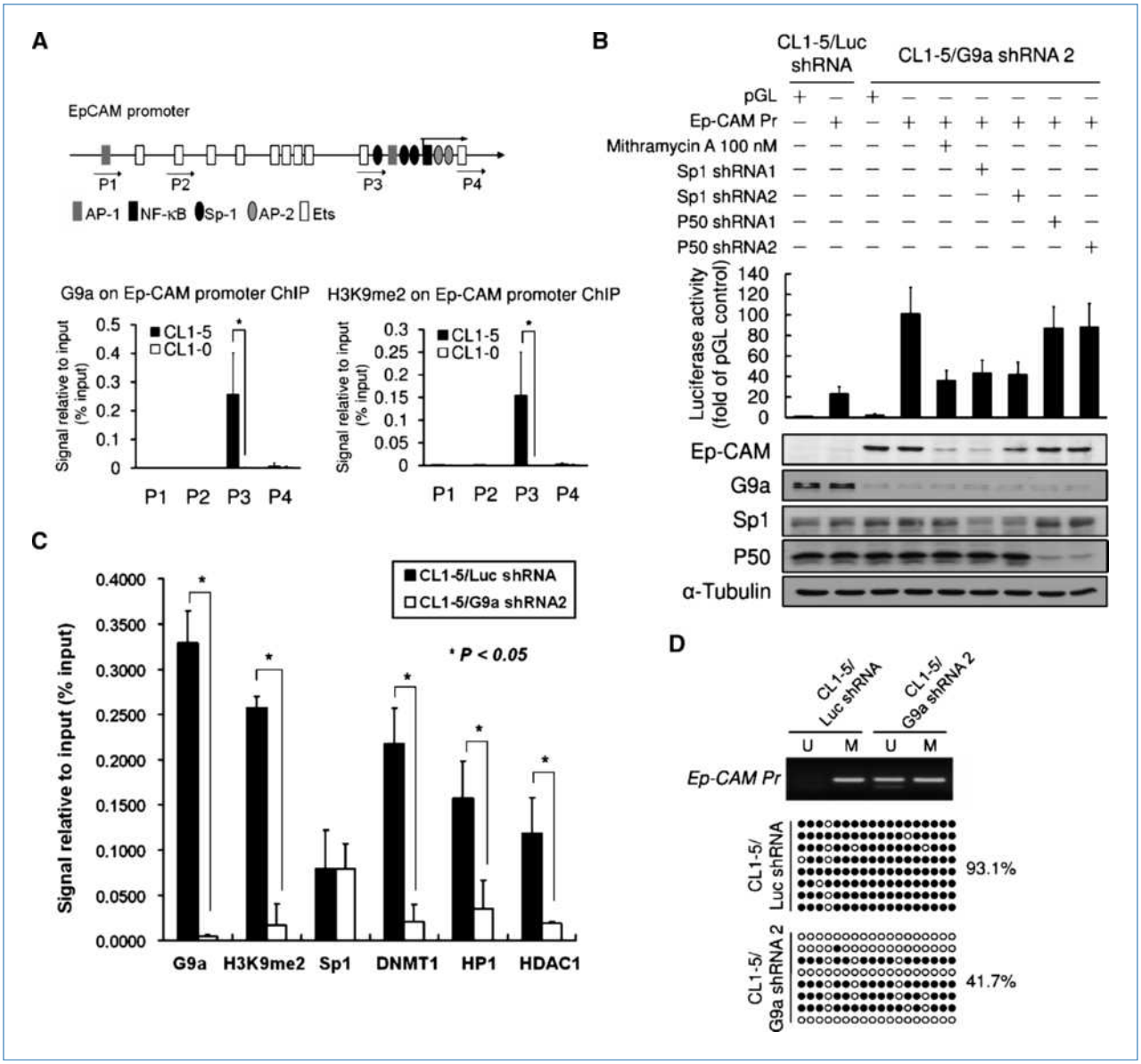

Figure 5. G9a induces the assembly of a repressor complex on the *Ep-CAM* promoter. A, top, schematic diagram of the human *Ep-CAM* promoter (GenBank accession no. AY148099). Arrow with numbers indicates the primer sets that were used for the ChIP analysis. Bottom, binding of G9a and H3K9me2 to the *Ep-CAM* promoter was determined by ChIP assay in CL1-5 and CL1-0 cells. B, G9a knockdown–mediated *Ep-CAM* gene transactivation requires Sp1. The fold increase in activation is shown above the bars, along with the plasmids transfected. C, ChIP analysis of the association of various regulatory factors with the *Ep-CAM* promoter region in CL1-5/Luc shRNA and CL1-5/G9a shRNA cells. D, top, changes in the DNA methylation status of the *Ep-CAM* promoter in CL1-5/Luc shRNA and G9a shRNA2 cells, as determined by MS-PCR. M, methylated DNA; U, unmethylated DNA. Bottom, bisulfite sequencing analysis of the *Ep-CAM* promoter in CL1-5/Luc shRNA and CL1-5/G9a shRNA2 cells. Filled circles, methylated CG; open circles, ummethylated CG. The methylation rate in each region (as a percentage) is indicated.

It is reported that G9a and GLP form a stoichiometric heteromeric complex *in vivo* and function cooperatively rather than redundantly to mediate H3K9 dimethylation at euchromatin (32, 42). Their interaction also stabilizes G9a protein from degradation. We tested the possibility that downregulation of GLP results in a similar phenotype as that observed with downregulation of G9a. We found that knockdown of GLP resulted in migration defect, as in the case of knockdown of G9a (Supplementary Fig. S11). Similar to the result of a previous report (17), GLP depletion also caused G9a protein depletion (Supplementary Fig. S13). Depletion of each protein will affect the function of the G9a-GLP complex. Collectively, our results indicate that downregulation of GLP results in a similar phenotype as that observed with downregulation of G9a. The results also suggest that GLP is essential in the promotion of cell migration by G9a.

In this study, we have provided substantial evidence linking G9a expression with lung cancer progression; however, the possible mechanisms of G9a overexpression associated with lung cancer metastasis remain elusive. Our preliminary data suggest that posttranslational regulation mechanisms may be involved. We have found that G9a expression is higher in lung tumor tissues compared with matched normal tissues (Supplementary Fig. S1). Local invasion is one of the early events for tumor metastasis. We have provided evidence to show that expression of G9a increases cell invasion (Fig. 2B). Taken together, increased expression of G9a may occur as an early event in metastasis processes. Other possibilities may also exist and cannot be ruled out at this moment. Recently, cancer stem cell is believed to act like a seed to metastasize at distant organ on entry into circulation. Indeed, we also found that G9a expression was higher in colon cancer stem cells (sorting against multiple colon stem cell markers such as CD133 and CD44), although this was not observed in our lung cancer cell models. Therefore, it is possible that high G9a expressing cells may contain more cancer stem cell potentials with higher capability for metastasis. Currently, the association between G9a expression and cancer stem cells is under investigation in our laboratory.

Our results showed that knockdown of Ep-CAM partially reversed metastasis suppression due to G9a knockdown *in vivo*. Furthermore, we showed that patients with high expression of G9a and with concomitantly low Ep-CAM levels had significantly shorter survival time in lung cancer TMA (Supplementary Fig. S8B). These findings are quite interesting and warrant further investigation because Ep-CAM is only one member of a large cohort of metastasis-relevant genes that may be repressed by G9a. Ep-CAM is a 40-kDa epithelial transmembrane glycoprotein that is abundantly present in most epithelial tissues and functions as a homophilic Ca^{2+}-independent cell-cell adhesion molecule (43). Loss of membranous Ep-CAM is associated with nuclear β-catenin localization and contributes to reduced cell-cell adhesions, increased migratory potential, and tumor budding (44). Nuclear translocation of β-catenin may cause activation of genes that are regulated by β-catenin. These studies may partially explain why Ep-CAM induces the reversal of G9a-mediated phenotypes. This supports the hypothesis that G9a may act via the pleiotropic regulation of multiple effectors.

In conclusions, we show that G9a is endowed with methyltransferase activity to concomitantly repress the downstream effector Ep-CAM, thereby promoting the invasion step of the invasion-metastasis cascade. Moreover, G9a levels correlate with reduced overall survival and disease-free interval, potentially representing an independent prognostic factor.

Disclosure of Potential Conflicts of Interest

No potential conflicts of interest were disclosed.

Acknowledgments

We thank Dr. Marianne Rots (University of Groningen) for the P39E plasmid and Dr. Kenneth L. Wright (University of South Florida) for DN-G9a and HA-G9a plasmids.

Grant Support

National Science Council, Taiwan (NSC97-2323-B-002-001) and Department of Health, Taiwan (DOH99-TD-C-111-004).

The costs of publication of this article were defrayed in part by the payment of page charges. This article must therefore be hereby marked *advertisement* in accordance with 18 U.S.C. Section 1734 solely to indicate this fact.

Received 03/09/2010; revised 07/12/2010; accepted 08/05/2010; published OnlineFirst 10/12/2010.

References

1. Jones PA, Baylin SB. The fundamental role of epigenetic events in cancer. Nat Rev Genet 2002;3:415–28.
2. Robertson KD. DNA methylation, methyltransferases, and cancer. Oncogene 2001;20:3139–55.
3. Pruitt K, Zinn RL, Ohm JE, et al. Inhibition of SIRT1 reactivates silenced cancer genes without loss of promoter DNA hypermethylation. PLoS Genet 2006;2:e40.
4. Fraga MF, Ballestar E, Villar-Garea A, et al. Loss of acetylation at Lys16 and trimethylation at Lys20 of histone H4 is a common hallmark of human cancer. Nat Genet 2005;37:391–400.
5. Ballestar E, Paz MF, Valle L, et al. Methyl-CpG binding proteins identify novel sites of epigenetic inactivation in human cancer. EMBO J 2003;22:6335–45.
6. Fahrner JA, Eguchi S, Herman JG, Baylin SB. Dependence of histone modifications and gene expression on DNA hypermethylation in cancer. Cancer Res 2002;62:7213–8.
7. Nguyen CT, Gonzales FA, Jones PA. Altered chromatin structure associated with methylation-induced gene silencing in cancer cells: correlation of accessibility, methylation, MeCP2 binding and acetylation. Nucleic Acids Res 2001;29:4598–606.
8. Dong KB, Maksakova IA, Mohn F, et al. DNA methylation in ES cells requires the lysine methyltransferase G9a but not its catalytic activity. EMBO J 2008;27:2691–701.
9. Ikegami K, Iwatani M, Suzuki M, et al. Genome-wide and locus-specific DNA hypomethylation in G9a deficient mouse embryonic stem cells. Genes Cells 2007;12:1–11.
10. Bachman KE, Park BH, Rhee I, et al. Histone modifications and silencing prior to DNA methylation of a tumor suppressor gene. Cancer Cell 2003;3:89–95.
11. Wozniak RJ, Klimecki WT, Lau SS, Feinstein Y, Futscher BW. 5-Aza-2′-deoxycytidine-mediated reductions in G9A histone methyltransferase and histone H3 K9 di-methylation levels are linked to tumor suppressor gene reactivation. Oncogene 2007;26:77–90.
12. Seligson DB, Horvath S, Shi T, et al. Global histone modification patterns predict risk of prostate cancer recurrence. Nature 2005;435:1262–6.
13. Park YS, Jin MY, Kim YJ, Yook JH, Kim BS, Jang SJ. The global histone modification pattern correlates with cancer recurrence and overall survival in gastric adenocarcinoma. Ann Surg Oncol 2008;15:1968–76.
14. Wei Y, Xia W, Zhang Z, et al. Loss of trimethylation at lysine 27 of histone H3 is a predictor of poor outcome in breast, ovarian, and pancreatic cancers. Mol Carcinog 2008;47:701–6.
15. Tachibana M, Sugimoto K, Fukushima T, Shinkai Y. Set domain-containing protein, G9a, is a novel lysine-preferring mammalian histone methyltransferase with hyperactivity and specific selectivity to lysines 9 and 27 of histone H3. J Biol Chem 2001;276:25309–17.

16. Rice JC, Briggs SD, Ueberheide B, et al. Histone methyltransferases direct different degrees of methylation to define distinct chromatin domains. Mol Cell 2003;12:1591–8.
17. Tachibana M, Sugimoto K, Nozaki M, et al. G9a histone methyltransferase plays a dominant role in euchromatic histone H3 lysine 9 methylation and is essential for early embryogenesis. Genes Dev 2002;16:1779–91.
18. Simon JA, Lange CA. Roles of the EZH2 histone methyltransferase in cancer epigenetics. Mutat Res 2008;647:21–9.
19. Kirmizis A, Bartley SM, Farnham PJ. Identification of the polycomb group protein SU(Z)12 as a potential molecular target for human cancer therapy. Mol Cancer Ther 2003;2:113–21.
20. Kondo Y, Shen L, Suzuki S, et al. Alterations of DNA methylation and histone modifications contribute to gene silencing in hepatocellular carcinomas. Hepatol Res 2007;37:974–83.
21. Watanabe H, Soejima K, Yasuda H, et al. Deregulation of histone lysine methyltransferases contributes to oncogenic transformation of human bronchoepithelial cells. Cancer Cell Int 2008;8:15.
22. Kondo Y, Shen L, Ahmed S, et al. Downregulation of histone H3 lysine 9 methyltransferase G9a induces centrosome disruption and chromosome instability in cancer cells. PLoS ONE 2008;3:e2037.
23. Steeg PS. Metastasis suppressors alter the signal transduction of cancer cells. Nat Rev Cancer 2003;3:55–63.
24. Bryant RJ, Cross NA, Eaton CL, Hamdy FC, Cunliffe VT. EZH2 promotes proliferation and invasiveness of prostate cancer cells. Prostate 2007;67:547–56.
25. Choi JH, Song YS, Yoon JS, Song KW, Lee YY. Enhancer of zeste homolog 2 expression is associated with tumor cell proliferation and metastasis in gastric cancer. APMIS 2010;118:196–202.
26. Min J, Zaslavsky A, Fedele G, et al. An oncogene-tumor suppressor cascade drives metastatic prostate cancer by coordinately activating Ras and nuclear factor-κB. Nat Med 2010;16:286–94.
27. Sobin LH, Fleming ID. TNM classification of malignant tumors, fifth edition (1997). Union Internationale Contre le Cancer and the American Joint Committee on Cancer. Cancer 1997;80:1803–4.
28. Chu YW, Yang PC, Yang SC, et al. Selection of invasive and metastatic subpopulations from a human lung adenocarcinoma cell line. Am J Respir Cell Mol Biol 1997;17:353–60.
29. Onn A, Isobe T, Itasaka S, et al. Development of an orthotopic model to study the biology and therapy of primary human lung cancer in nude mice. Clin Cancer Res 2003;9:5532–9.
30. Tai KY, Shiah SG, Shieh YS, et al. DNA methylation and histone modification regulate silencing of epithelial cell adhesion molecule for tumor invasion and progression. Oncogene 2007;26:3989–97.
31. Dobrovic A, Bianco T, Tan LW, Sanders T, Hussey D. Screening for and analysis of methylation differences using methylation-sensitive single-strand conformation analysis. Methods 2002;27:134–8.
32. Tachibana M, Ueda J, Fukuda M, et al. Histone methyltransferases G9a and GLP form heteromeric complexes and are both crucial for methylation of euchromatin at H3–9. Genes Dev 2005;19:815–26.
33. Zhang X, Tamaru H, Khan SI, et al. Structure of the Neurospora SET domain protein DIM-5, a histone H3 lysine methyltransferase. Cell 2002;111:117–27.
34. Zhang X, Yang Z, Khan SI, et al. Structural basis for the product specificity of histone lysine methyltransferases. Mol Cell 2003;12:177–85.
35. McLaughlin PM, Trzpis M, Kroesen BJ, et al. Use of the EGP-2/Ep-CAM promoter for targeted expression of heterologous genes in carcinoma derived cell lines. Cancer Gene Ther 2004;11:603–12.
36. Seligson DB, Horvath S, McBrian MA, et al. Global levels of histone modifications predict prognosis in different cancers. Am J Pathol 2009;174:1619–28.
37. Ellinger J, Kahl P, von der Gathen J, et al. Global levels of histone modifications predict prostate cancer recurrence. Prostate 2010;70:61–9.
38. Ng SS, Kavanagh KL, McDonough MA, et al. Crystal structures of histone demethylase JMJD2A reveal basis for substrate specificity. Nature 2007;448:87–91.
39. Cloos PA, Christensen J, Agger K, et al. The putative oncogene GASC1 demethylates tri- and dimethylated lysine 9 on histone H3. Nature 2006;442:307–11.
40. Shi Y, Lan F, Matson C, et al. Histone demethylation mediated by the nuclear amine oxidase homolog LSD1. Cell 2004;119:941–53.
41. Tachibana M, Matsumura Y, Fukuda M, Kimura H, Shinkai Y. G9a/GLP complexes independently mediate H3K9 and DNA methylation to silence transcription. EMBO J 2008;27:2681–90.
42. Ueda J, Tachibana M, Ikura T, Shinkai Y. Zinc finger protein Wiz links G9a/GLP histone methyltransferases to the co-repressor molecule CtBP. J Biol Chem 2006;281:20120–8.
43. Litvinov SV, Velders MP, Bakker HA, Fleuren GJ, Warnaar SO. Ep-CAM: a human epithelial antigen is a homophilic cell-cell adhesion molecule. J Cell Biol 1994;125:437–46.
44. Gosens MJ, van Kempen LC, van de Velde CJ, van Krieken JH, Nagtegaal ID. Loss of membranous Ep-CAM in budding colorectal carcinoma cells. Mod Pathol 2007;20:221–32.